

Article

Stefan Blowing Impacts on Hybrid Nanofluid Flow over a Moving Thin Needle with Thermal Radiation and MHD

Vinodh Srinivasa Reddy ¹, Jagan Kandasamy ¹ and Sivasankaran Sivanandam ^{2,*}

¹ Department of Mathematics, School of Engineering, Presidency University, Bangalore 560064, India; vinodh.ks@presidencyuniversity.in (V.S.R.); kjaganppmaths@gmail.com (J.K.)

² Mathematical Modelling and Applied Computation Research Group, Department of Mathematics, King Abdulaziz University, Jeddah 21589, Saudi Arabia

* Correspondence: sd.siva@yahoo.com or smsivanandam@kau.edu.sa

Abstract: This investigation focuses on the impact of Stefan blowing on the flow of hybrid nanofluids over a moving slender needle with magnetohydrodynamics (MHD), thermal radiation, and entropy generation. To facilitate analysis, suitable transformations are applied to convert the governing partial differential equations into a set of ordinary differential equations, which are then solved analytically using Homotopy Analysis Method (HAM) in Mathematica. This study investigates how varying the values of Stefan blowing, magnetic field, and thermal radiation parameters impact the profiles of velocity, temperature, and concentration. Additionally, the study analyzes the outcomes of the local skin friction, local Nusselt number, and local Sherwood number. Increasing the magnetic field reduces the velocity profile. The temperature profile is enhanced by a rise in the thermal radiation parameter. Also, the results reveal that an increase in the Stefan blowing number leads to higher profiles of velocity.

Keywords: hybrid nanofluid; Stefan blowing; MHD; thermal radiation; thin needle; entropy generation



Citation: Reddy, V.S.; Kandasamy, J.; Sivanandam, S. Stefan Blowing Impacts on Hybrid Nanofluid Flow over a Moving Thin Needle with Thermal Radiation and MHD. *Computation* **2023**, *11*, 128. <https://doi.org/10.3390/computation11070128>

Academic Editor: Sergey A. Karabasov

Received: 21 May 2023

Revised: 13 June 2023

Accepted: 27 June 2023

Published: 29 June 2023



Copyright: © 2023 by the authors. Licensee MDPI, Basel, Switzerland. This article is an open access article distributed under the terms and conditions of the Creative Commons Attribution (CC BY) license (<https://creativecommons.org/licenses/by/4.0/>).

1. Introduction

Smart fluids, known as hybrid nanofluids, contain suspensions of two or more different types of nanoparticles in the base fluid, significantly improving their characteristics even at low concentrations. They have a lot of potential and are used in solar collectors, heat exchangers, refrigerators, desalination, electrical and engine cooling, machining, and heat transfer. Siti et al. [1] conducted a study in which they analyzed the flow characteristics of a horizontal thin needle submerged in a nanofluid under steady 2D laminar forced convection. Ghadikolaei et al. [2] investigated the thermophysical properties of hybrid nanofluid transport, focusing on the influence of the shape factor in stagnation point flow. The effects of the mixed convection parameters, needle size on the flow of fluid, and the heat transfer characteristics of moving a vertical thin needle in nanofluid were investigated by Siti et al. [3]. Iskandar et al. [4] conducted research that focused on studying the steady motion and heat transfer characteristics of a permeable slender moving needle over a hybrid nanofluid. Waqas et al. [5] investigated the effects of velocity slip and nonlinear thermal radiation on a MoS₄-Ag/engine-oil base hybrid nanofluid containing SWCNTs and MWCNTs, set up in a vertical cylinder. The influence of suction and unsteadiness parameters on the motion and heat transfer characteristics of a hybrid nanofluid over a permeable shrinking cylinder was examined by Zainal et al. [6]. The convective flow of nanofluids/hybrid nanofluids under various situations has been examined in several studies [7–10].

MHD is a field of study that focusses on the interaction of magnetic fields with electrically conductive fluids, such as plasma and molten metals [11,12]. MHD finds various applications across different fluids, including power generation, nuclear fusion, space propulsion, material processing, astrophysics and space science, and environmental

and biomedical applications [13,14]. Sulochana et al. [15] conducted an investigation on the boundary layer theory for 2D forced convection flow along a moving thin needle with joule heating and an MHD radiative nanoliquid. The MHD bioconvective flow of a nanoliquid in a stratified medium, with consideration of gyrotactic microorganisms, was investigated by Jagan et al. [16]. The objective of the study conducted by Khan et al. [17] was to assess the impact of nonlinear radiation on the magnetic field using hybrid AA7075 and AA7072 alloy nanomaterials. In their research, Iskander et al. [18] explored the flow and energy transport of a hybrid nanofluid induced by a persistently moving needle in an MHD Sakiadis flow with resistive heating. In a study conducted by Reddy et al. [19], the research focused on investigating the flow of a hybrid nanoliquid over a moving thin needle with MHD while also investigating the impacts of Dufour and Soret effects using the Casson model.

Thermal radiation refers to the emission of energy in the form of electromagnetic radiation from a heated surface, which propagates in all directions at the speed of light until it is observed at its point of absorption. The ability to control thermal radiation is crucial in various applications, including thermal management, spectroscopy, optoelectronics, and energy-conversion devices [20,21]. In their research, Karthikeyan et al. [22] carried out an extensive study on unsteady MHD conducting fluid past a semi-infinite vertical plate situated within a porous medium, considering time-dependent suction. Niranjana et al. [23] conducted a research study to examine the impact of Soret and Dufour effects on the MHD flow of a viscous fluid towards a vertical plate embedded in a porous medium with a primary focus on slip and chemical reaction. In their research, Iskander et al. [24] studied how the characteristics of the flow of dissipative nanofluids are affected by nonlinear thermal radiation when they pass a thin, moving needle on a horizontal plane. In their study, Himanshu et al. [25] examined the effects of non-linear thermal radiation, Joule heating, and viscous dissipation on the flow of an MHD nanoliquid over a moving slender needle. In the research article conducted by Sreedevi et al. [26], they studied the effects of nonlinear thermal radiation and the Biot number on the flow along a continuously moving slender needle filled with carbon-based nanotubes. In their research article, Makinde et al. [27] investigated the bioconvection behavior of a radiating hybrid nanoliquid flowing past a thin needle while considering the impacts of a heterogeneous-homogeneous chemical reaction. Haider et al. [28] investigated the influence of the effects of blowing on the unsteady MHD flow of a nanoliquid over a stretching sheet, taking into account the effects of Arrhenius activation energy, thermal radiation, and chemical reaction.

The Stefan blowing effect, which establishes a direct proportionality between the species (concentration) field and velocity field, is commonly observed in various applications such as the drying process for paper and the blowing of glass, among others [29]. Tiegang et al. [30] conducted a research study to analyze the effects of blowing on mass transfer in high flux conditions while investigating the flow, heat, and mass transfer of a viscous fluid over a stretching sheet. Giri et al. [31] explored the influence of Stefan blowing on hydro-magnetic bioconvection by studying the behavior of a water-based nanoliquid containing gyrotactic microorganisms over a permeable surface. Additionally, Amirson et al. [32] developed a transport model in their research article to describe the behavior of an MHD forced convective non-Newtonian boundary flow from a thin needle in a nanofluid, taking into consideration the effects of Stefan blowing and microorganisms and ensuring the originality of the content. The effects of Stefan blowing, Dufour and Soret effects, thermophoresis, and Brownian motion on Casson liquid flow past a moving thin needle were studied by Jyothi et al. [33]. Narayanaswamy et al. [34] conducted a study on the thermal radiation, Dufour effect, and Soret effect over a stretching cylinder with Stefan blowing.

Entropy generation is a measure of the amount of energy that is wasted during the process. This can include things like heat transfer, fluid flow, and chemical reactions. Also, it is a measure of randomness in a system, and it is always greater than or equal to zero. The objective of Afridi et al. [35] was to investigate and compare the generation of entropy in the flow of conventional and hybrid nanofluids. In their study, Tlili et al. [36]

examined the characteristics of a two-dimensional MHD nanofluid flow involving water-based suspended carbon nanotubes. The investigation included the analysis of entropy generation and nonlinear thermal radiation, within a Darcy-Forchheimer porous medium, over a horizontally moving thin needle. In their research, Gangadhar et al. [37] conducted an analysis focused on thermal optimization in magnetic materials. The study examined the entropy generation within a mixed convective MHD flow, specifically considering an electrically conductive nanoliquid containing motile microorganisms in conjunction with a vertical cylinder. Ramzan et al. [38] conducted a comprehensive investigation into the mechanical characteristics of heat and mass transfer flow in a second-grade nanofluid. Additionally, they analyzed the motion of gyrotatic microorganisms past a thin needle with the dipole effect, taking into account entropy generation and thermal radiation. Ogunseye et al. [39] aimed to numerically examine the generation of entropy, heat propagation, and conduction in a hybridized Casson ferrofluid with dissipation and radiation, specifically within a thin needle.

In this study, we conducted an investigation to analyze the impacts of Stefan blowing on the flow behavior of a hybrid nanofluid over a moving thin needle while considering the effects of MHD, entropy generation, and thermal radiation. To the best of our knowledge, the impacts of Stefan blowing on the flow of a hybrid nanoliquid over a slender moving needle with MHD, thermal radiation, and entropy generation have not been explored in the existing literature. The HAM implemented in Mathematica software was employed to solve the problem at hand. The findings of this study are presented through tables and graphs, which illustrate the significant variations of various physical quantities with respect to the parameters under consideration. The findings of this study carry practical implications across various fields such as cooling technology, physics, and engineering, as well as thermal science.

2. Mathematical Formulation

The section provides the hybrid nanofluid’s physical model and governing equations. Figure 1 illustrates the physical model of a steady, incompressible, and laminar flow of a hybrid nanoliquid over a moving slender needle in this regard. The axial and radial coordinates are taken as the cylindrical coordinates in this instance, which are x and r , respectively. The boundary layer over the needle in this instance is not thicker than it. The free stream velocity U_∞ and the needle velocity U_w will move in the axial direction of fluid flow. In addition, a perpendicular to the flow direction magnetic field is applied. The concentrations at the wall and in the vicinity are also considered to be constant. Furthermore, the following terms: MHD, thermal radiation, and Stefan blowing effect, are included in the fundamental equations.

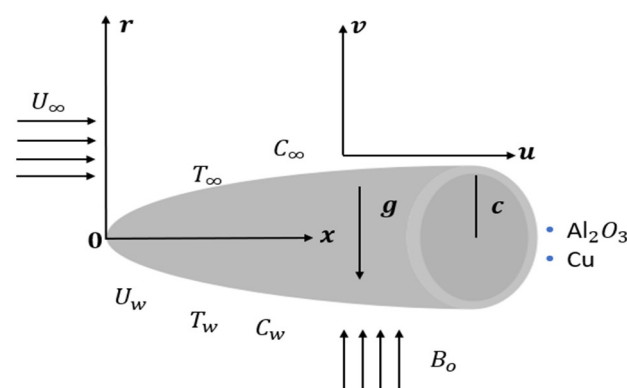


Figure 1. Physical diagram.

The governing equations of this study have been formulated based on (Sulochana et al. [15] and Jyothi et al. [33]), as provided in the list below.

$$\frac{\partial(ru)}{\partial x} + \frac{\partial(rv)}{\partial r} = 0 \tag{1}$$

$$u \frac{\partial u}{\partial x} + v \frac{\partial u}{\partial r} = \frac{\mu_{hnf}}{\rho_{hnf}} \frac{1}{r} \frac{\partial}{\partial r} \left(r \frac{\partial u}{\partial r} \right) - \frac{\sigma_{hnf} B_0^2 u}{\rho_{hnf}} \tag{2}$$

$$u \frac{\partial T}{\partial x} + v \frac{\partial T}{\partial r} = \frac{k_{hnf}}{(\rho C_p)_{hnf}} \frac{1}{r} \frac{\partial}{\partial r} \left(r \frac{\partial T}{\partial r} \right) - \frac{1}{(\rho C_p)_{hnf}} \frac{1}{r} \frac{\partial}{\partial r} (r q_r) + \frac{\sigma_{hnf}}{(\rho C_p)_{hnf}} B_0^2 u^2 \tag{3}$$

$$u \frac{\partial C}{\partial x} + v \frac{\partial C}{\partial r} = \frac{D_m}{r} \frac{\partial}{\partial r} \left(r \frac{\partial C}{\partial r} \right) \tag{4}$$

Associated boundary conditions are subjected to (Jyothi et al. [33]).

$$\left. \begin{aligned} u = u_w, v = \frac{-D_m}{(1-C_w)} \frac{\partial C}{\partial r}, T = T_w, C = C_w \text{ at } r = R(x) \\ u \rightarrow u_\infty, C \rightarrow C_\infty, T \rightarrow T_\infty \text{ as } r \rightarrow \infty \end{aligned} \right\} \tag{5}$$

The velocity components along the x and r axes are represented by u and v , respectively, in the given equations. Detailed information regarding the thermophysical properties of the nanoparticles and base fluid can be found in Tables 1 and 2, respectively. ϕ_1 and ϕ_2 stand for Al_2O_3 and copper nanoparticles, respectively, in terms of volume fraction.

Table 1. The thermophysical properties of the hybrid nanofluid employed in this research are as follows (Iskandar et al. [4] and Narayanaswamy et al. [29]).

| Properties | Hybrid Nanofluid |
|-------------------------|--|
| Density | $\rho_{hnf} = [\phi_1 \rho_{s1} + (1 - \phi_2) \rho_f] (1 - \phi_1) + \phi_2 \rho_{s2}$ |
| Heat capacity | $(\rho C_p)_{hnf} = [(1 - \phi_2) (\rho C_p)_f + \phi_1 (\rho C_p)_{s1}] (1 - \phi_1) + \phi_2 (\rho C_p)_{s2}$ |
| Dynamic viscosity | $\mu_{hnf} = \frac{\mu_f}{(1 - \phi_1)^{2.5} (1 - \phi_2)^{2.5}}$ |
| Thermal conductivity | $\frac{k_{hnf}}{k_f} = \frac{k_{s2} + k_{nf} (2 - 2\phi_2) + 2\phi_2 k_{s2}}{k_{s2} - \phi_2 k_{s2} + k_{nf} (2 + \phi_2)}$ Where $k_{nf} = \frac{k_{s1} + 2k_f - 2\phi_1 (k_f - k_{s1})}{k_{s1} + 2k_f + \phi_1 (k_f - k_{s1})} k_f$ |
| Electrical Conductivity | $\frac{\sigma_{hnf}}{\sigma_f} = \frac{\sigma_{s2} + \sigma_{nf} (2 - 2\phi_2) + 2\phi_2 \sigma_{s2}}{\sigma_{s2} - \phi_2 \sigma_{s2} + \sigma_{nf} (2 + \phi_2)}$ Where $\sigma_{nf} = \frac{\sigma_{s1} + 2\sigma_f - 2\phi_1 (\sigma_f - \sigma_{s1})}{\sigma_{s1} + 2\sigma_f + \phi_1 (\sigma_f - \sigma_{s1})} \sigma_f$ |

Table 2. The thermophysical properties of nanoparticles and base fluid are considered in this research (Iskandar et al. [4] and Narayanaswamy et al. [29]).

| Properties | Al_2O_3 | Cu | Water |
|--------------------------|-------------------------|--------------------|--------------------|
| $\sigma (\Omega m^{-1})$ | 1.502×10^{-10} | 5.96×10^7 | 5×10^{-2} |
| $k (W m^{-1} K^{-1})$ | 40 | 400 | 0.613 |
| $C_p (J kg^{-1} K^{-1})$ | 765 | 385 | 4179 |
| $\rho (kg m^{-3})$ | 3970 | 8933 | 997.1 |

The similarity variables and stream functions for the formulated governing equations are provided below (Jyothi et al. [22]).

$$\varphi = \nu_f x f(\eta), \theta(\eta) = \frac{T - T_\infty}{T_w - T_\infty}, \eta = \frac{Ur^2}{\nu_f x}, \phi(\eta) = \frac{C - C_\infty}{C_w - C_\infty} \tag{6}$$

By using the above transformations (6), Equation (1) is satisfied, and the nonlinear PDE Equations (2)–(5) are converted into nonlinear ODE Equations (7)–(10),

$$\frac{2}{B_1 B_2} (\eta f''' + f'') + f f'' - \frac{B_3}{B_2} M f' = 0 \tag{7}$$

$$\frac{2}{Pr C_2} (C_1 + \frac{4}{3} Rd) (\theta' + \eta \theta'') + f \theta' + \frac{B_3}{C_2} M Ec f'^2 = 0 \tag{8}$$

$$\frac{2}{Sc} (\phi' + \eta \phi'') + f \phi' = 0 \tag{9}$$

subjected to

$$\left. \begin{aligned} f(\eta) = 2\eta \frac{Sb}{Sc} \phi'(\eta) + \frac{\epsilon}{2} \eta, f'(\eta) = \frac{1}{2} \epsilon, \theta(\eta) = 1, \phi(\eta) = 1 \text{ at } \eta = c \\ f'(\eta) = \frac{1}{2} (1 - \epsilon), \phi(\eta) \rightarrow 0, \theta(\eta) \rightarrow 0 \text{ as } \eta \rightarrow \infty \end{aligned} \right\} \tag{10}$$

where $B_1 = \frac{\mu_f}{\mu_{mf}}, B_2 = \frac{\rho_{lmf}}{\rho_f}, B_3 = \frac{\sigma_{lmf}}{\sigma_f}, B_4 = \frac{k_{lmf}}{k_f}$ and $B_5 = \frac{(\rho C_p)_{lmf}}{(\rho C_p)_f}$ are the constants. $\nu_f = \frac{\mu_f}{\rho_f}, Pr = \frac{(\mu C_p)_f}{k_f}, M = \frac{\sigma_f B_0^2 x}{2u\rho_f}, Sb = \frac{(1-C_w)}{(C_w-C_\infty)}, \epsilon = \frac{U_w}{U}, Ec = \frac{(2u)^2}{(C_p)_f(T_w - T_\infty)}, Sc = \frac{\nu_f}{D_m}$ and $Rd = \frac{4\sigma^* T_\infty^3}{k^* k_f}$ represents the parameters of kinematic viscosity, Prandtl number, magnetic field, Stefan blowing, velocity ratio, Eckert number, Schmidt number, and thermal radiation, respectively.

Listed below are the relevant physical parameters: the skin friction coefficient, local Nusselt number, and local Sherwood number.

$$C_f = \frac{4C^{1/2}}{B_1} (Re_x)^{-1/2} f''(c) \tag{11}$$

$$Nu_x = -2C^{1/2} (C_1 + \frac{4}{3} Rd) (Re_x)^{1/2} \theta'(c) \tag{12}$$

$$Sh_x = -2C^{1/2} (Re_x)^{1/2} \phi'(c) \tag{13}$$

where $Re_x = \frac{Ux}{\nu_f}$ is the local Reynolds number.

3. Entropy Generation

The current investigation allows us to depict the rate of volumetric entropy generation as (Muhammed et al. [35] and Gangadhar et al. [37]).

$$Ec = \frac{k_f}{T_\infty^2} \left[\frac{k_{lmf}}{k_f} + \frac{16\sigma^* T^3}{3k^* k_f} \right] \left(\frac{\partial T}{\partial r} \right)^2 + \frac{\sigma_{lmf} B_0^2}{T_\infty} u^2 + \frac{D_m}{C_\infty} \left(\frac{\partial C}{\partial r} \right)^2 + \frac{\mu_{lmf}}{T_\infty} \left(\frac{\partial u}{\partial r} \right)^2 \tag{14}$$

The generation of entropy (N_G) is determined by dividing the volumetric generation by the characteristic entropy generation:

$$N_G = \frac{E_G}{E_0}$$

The characteristic entropy generation is given by

$$E_0 = \frac{4 k_f U}{v_f x}$$

$$N_G = \left(C_1 + \frac{4}{3} Rd \right) \Lambda_1^2 \eta \theta'^2 + \frac{B_3}{2} Pr M Ec \Lambda_1 f'^2 + \Lambda_3 \Lambda_2' \eta \phi'^2 + \frac{Pr Ec \Lambda_1 \eta}{B_1} f'^2 \quad (15)$$

where, $\Lambda_1 = \frac{T_w - T_\infty}{T_\infty}$, $\Lambda_2 = \frac{C_w - C_\infty}{C_\infty}$ and $\Lambda_3 = \frac{R D_m (C_w - C_\infty)}{k_f}$ are the temperature difference parameter, concentration difference parameter, and diffusion parameter.

The Bejan number quantifies the ratio between the transfer of heat and mass and the overall entropy (Gangadhar et al. [37]).

$$Bn = \frac{\left(C_1 + \frac{4}{3} Rd \right) \Lambda_1^2 \eta \theta'^2 + \Lambda_3 \Lambda_2' \eta \phi'^2}{\left(C_1 + \frac{4}{3} Rd \right) \Lambda_1^2 \eta \theta'^2 + \frac{B_3}{2} Pr M Ec \Lambda_1 f'^2 + \Lambda_3 \Lambda_2' \eta \phi'^2 + \frac{Pr Ec \Lambda_1 \eta}{B_1} f'^2} \quad (16)$$

Therefore, based on Equation (16), the Bejan number (Bn) ranges from 0 and 1. When $Bn \gg 0.5$, indicates that the heat transfer predominately contributes to the irreversibility. Conversely, when $Bn \ll 0.5$, suggests that irreversibility is primarily caused by fluid friction, thermal radiation, and joule heating. When $Bn = 0.5$, it signifies that irreversibility arises equally from fluid friction, joule heating, heat, and mass transfer.

4. Method of Solution

HAM gives a series of solutions used to solve nonlinear problems. It is an iterative numerical technique that combines the benefits of both analytical and numerical methods [40]. It provides a systematic approach to solve problems that are not amenable to traditional analytical methods such as numerical integration or differential equations. It is based on the idea of the continuous deformation of the solutions of a problem until they reach the solutions of the original problem. One of the key benefits of HAM is its ability to provide a precise approximation of the solution to a nonlinear problem, particularly in instances when the exact solution is unknown [41,42]. The system of Equations (7)–(9) with boundary conditions (10) is solved using the HAM by carefully selecting appropriate initial approximations and auxiliary linear operators.

$$f_0(\eta) = -2 \frac{Sb}{Sc} c + (c + 1) \left(\frac{2\varepsilon - 1}{2} \right) + \left(\frac{1}{2} - \varepsilon \right) \eta + \left(\frac{1 - 2\varepsilon}{2} \right) \exp(c - \eta)$$

$$\theta_0(\eta) = \exp(c - \eta), \phi_0(\eta) = \exp(c - \eta)$$

$$L_f(f) = \frac{\partial^3 f}{\partial \eta^3} - \frac{\partial f}{\partial \eta}, L_\theta(\theta) = \frac{\partial^2 \theta}{\partial \eta^2} - \theta, L_\phi(\phi) = \frac{\partial^2 \phi}{\partial \eta^2} - \phi$$

which satisfies the property

$$L_f[E_1 + E_2 \exp(\eta) + E_3 \exp(-\eta)] = 0$$

$$L_\theta[E_4 \exp(\eta) + E_5 \exp(-\eta)] = 0$$

$$L_\phi[E_6 \exp(\eta) + E_7 \exp(-\eta)] = 0$$

where $E_1, E_2 \dots E_7$ are arbitrary constants.

The convergence of the series solution obtained through the HAM is evaluated using the h-curve, which incorporates the auxiliary parameters. These parameters play a pivotal role in adjusting the convergence of the HAM solutions. The curves of h_f , h_θ , and h_ϕ are presented in Figure 2. The h-curve is plotted for $\phi_1 = 0.15$, $\phi_2 = 0.15$, $M = 0.1$, $Pr = 6.2$, $Sc = 0.6$, $\varepsilon = 1$, $Sb = 0.5$, $Rd = 0.1$, $c = 0.1$, $Ec = 0.2$. As depicted in Figure 2, the admissible ranges of h_f , h_θ , and h_ϕ are $-0.4 \leq h_f \leq 0.1$, $-0.35 \leq h_\theta \leq 0.1$, and $-0.27 \leq h_\phi \leq 0.1$.

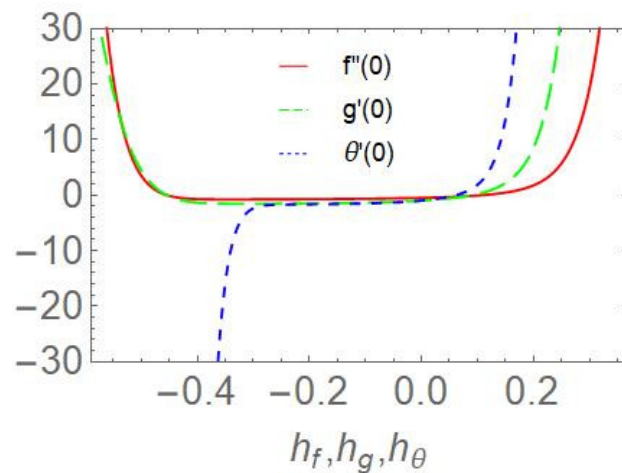


Figure 2. Displays the h-curves corresponding to h_f , h_θ , and h_ϕ .

5. Results and Discussion

In this study, the HAM is employed to analyze highly nonlinear and coupled Equations (7)–(9) that are subjected to corresponding boundary restrictions Equation (11). The study investigates various parameter combinations, including the variation of thermal radiation, magnetic field, and Stefan blowing parameters, as depicted in Figures 3–5. Figures 6–8 illustrate the analysis of local skin friction, Nusselt number, and Sherwood number while considering various values of magnetic field, Stefan blowing, and thermal radiation parameters. The variation of the Eckert number and diffusion parameters is depicted in Figure 9 for entropy generation. Table 3 shows the calculated results for M , Sb , and Rd .

Figure 3 shows the increasing magnetic field velocity profile decreases. As the magnetic field increases, it creates a Lorentz force on the electrons of the conductor, which opposes the flow of the fluid. This means that the electrons move slowly, and the velocity profile decreases.

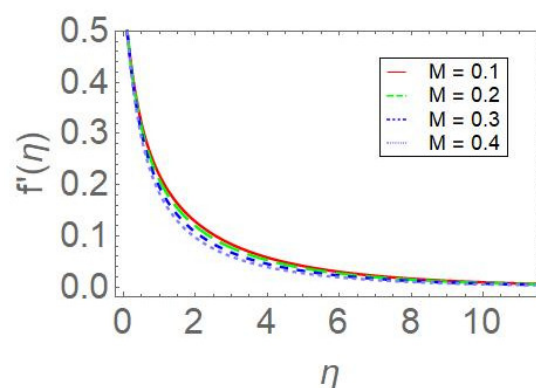


Figure 3. Effects of M on $f'(\eta)$.

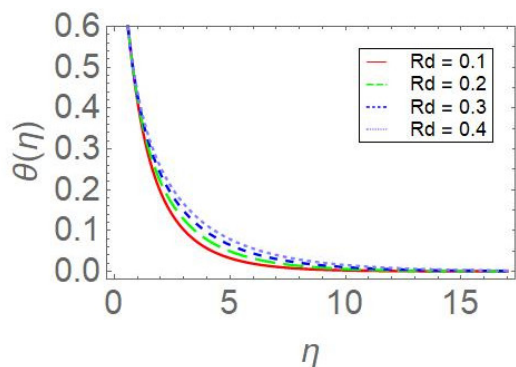


Figure 4. Impacts of Rd on $\theta(\eta)$.

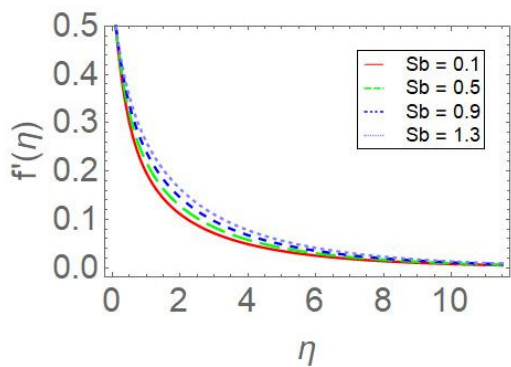
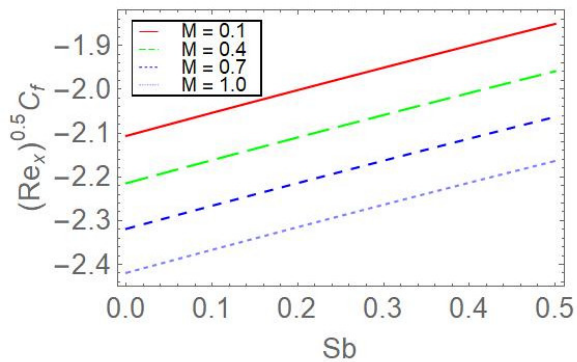
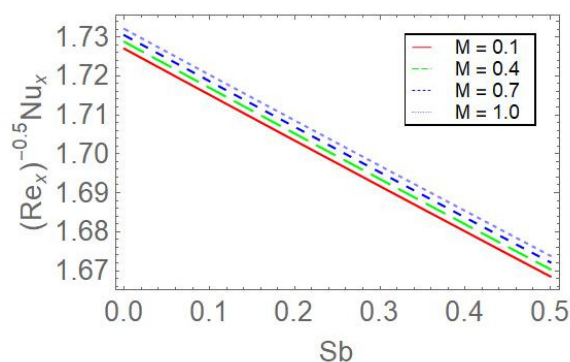


Figure 5. Effects of Sb on $f'(\eta)$.



(a)



(b)

Figure 6. Impacts of (a) M on $(Re_x)^{0.5} C_f$ and (b) M on $(Re_x)^{-0.5} Nu_x$.

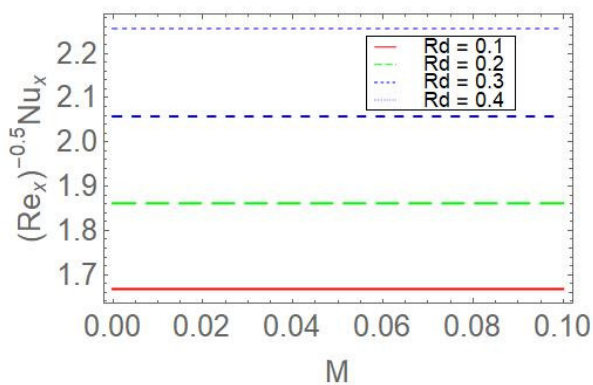


Figure 7. Impacts of Rd on $(Re_x)^{-0.5} Nu_x$.

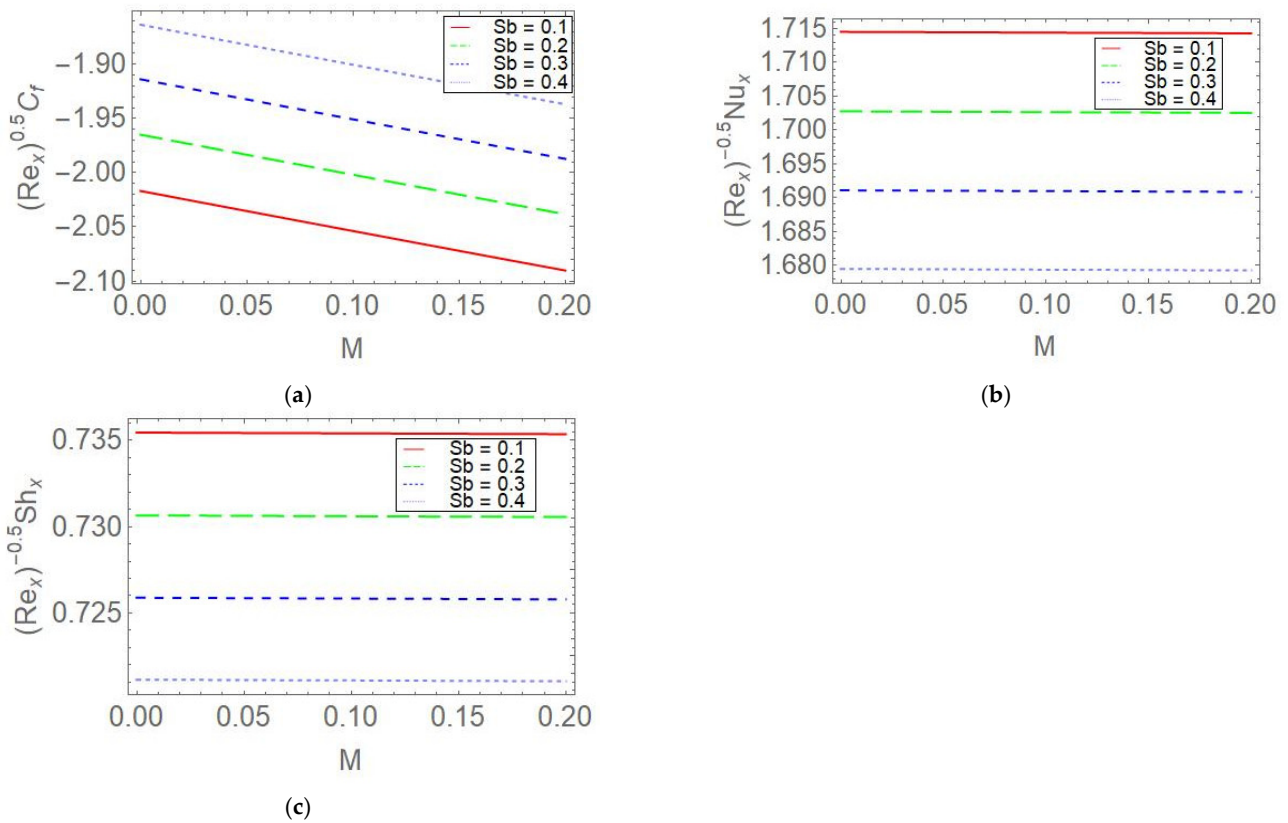


Figure 8. Influences of (a) Sb on $(Re_x)^{0.5} C_f$, (b) Sb on $(Re_x)^{-0.5} Nu_x$, and (c) Sb on $(Re_x)^{-0.5} Sh_x$.

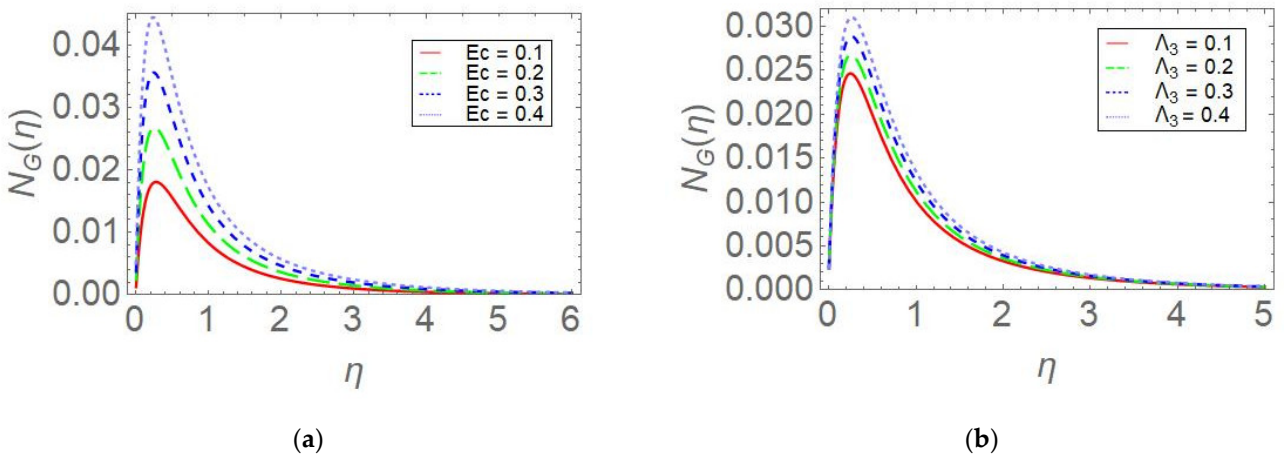


Figure 9. Effects of (a) Ec on $N_G(\eta)$ and (b) Λ_3 on $N_G(\eta)$.

Figure 4 represents the Rd temperature profile increases. Thermal radiation is a form of energy transfer, and as it increases, it will cause fluid to absorb more energy. This additional energy will cause the temperature of the fluid to increase. This increase in temperature will result in the temperature profile becoming more pronounced.

As shown in Figure 5, when the Sb increases, the velocity profile also increases. Stefan blowing is a process used to increase the velocity of a fluid by introducing additional energy. The additional energy causes the fluid to become more energetic, resulting in an increase in velocity of the fluid. This increases the velocity profile.

As shown in Figure 6a,b, increasing the values of M can decrease skin friction due to the suppression of fluid motion while simultaneously increasing the Nusselt number because of the enhanced convective heat transfer caused by the induced fluid motion.

Table 3. Computed results for different physical parameters Rd, M, and Sb.

| Rd | M | Sb | $C_f(\text{Re}_x)^{0.5}$ | $Nu_x(\text{Re}_x)^{-0.5}$ | $Sh_x(\text{Re}_x)^{-0.5}$ |
|-----|-----|-----|--------------------------|----------------------------|----------------------------|
| 0.1 | 0.1 | 0.5 | -1.94549 | 1.70681 | 0.74003 |
| | 0.4 | | -2.08484 | 1.70623 | 0.73979 |
| | 0.7 | | -2.21756 | 1.70568 | 0.73956 |
| | 1.0 | | -2.34425 | 1.70516 | 0.73935 |
| 0.1 | 0.1 | 0.1 | -2.05374 | 1.71442 | 0.73540 |
| | | 0.2 | -2.00182 | 1.70266 | 0.73060 |
| | | 0.3 | -1.9507 | 1.69096 | 0.72583 |
| | | 0.4 | -1.90036 | 1.67933 | 0.72109 |
| 0.1 | 0.1 | 0.5 | -1.8508 | 1.66777 | 0.71637 |
| 0.2 | | | -1.8508 | 1.86173 | 0.71637 |
| 0.3 | | | -1.8508 | 2.05793 | 0.71637 |
| 0.4 | | | -1.8508 | 2.25604 | 0.71637 |

Figure 7 shows that as Rd increases, the value of Nu_x also increases. The Nusselt number is used to measure the rate of convective heat transfer between a solid surface and the fluid surrounding it. An increase in the thermal radiation from the surface results in a rise in local temperature, leading to a higher temperature gradient between the surface and the surrounding fluid. This intensifies the temperature gradient and enhances convective heat transfer, causing the Nusselt number to increase.

In Figure 8a–c, C_f rises, but Nu_x and Sh_x fall. The increased flow rate of Stefan blowing causes the skin friction to increase because of the increased viscous forces between the flow and the wall. This in turn reduces the Nusselt number and Sherwood number since these numbers are inversely proportional to the skin friction. Therefore, when the skin friction increases, the Nusselt number and Sherwood number decrease.

As shown in Figure 9a,b, increasing the Eckert number leads to an increase in entropy generation. This is because higher Eckert numbers correspond to higher velocities and higher energy dissipation within the flow. Increasing the diffusion parameter increases mass diffusivity and reduces the density of the hybrid nanofluid, which creates a more disordered system. Hence, entropy generation is increased.

Table 3 displays the calculated values for M, Sb, and Rd. As the value of M is increased while keeping Sb constant, the skin friction, Nusselt number, and Sherwood number decrease. Similarly, when the value of Sb is increasing while keeping M constant, the skin friction rises to 7.45% but the Nusselt and Sherwood number declines to 2.08% and 1.94%. On the other hand, by increasing the value of Rd while keeping M constant, the Nusselt number can increase by up to 35%.

6. Conclusions

The effects of Stefan blowing on a hybrid nanofluid flow involving MHD, thermal radiation, and entropy generation over a slender moving needle were studied. Our findings were as follows:

- The range of motion of the velocity profile becomes restricted as the strength of the magnetic field increases.
- As the thermal radiation intensifies, the thermal boundary layer expands.
- Elevating the Stefan blowing parameter results in an increase in the profiles of velocity.
- Raising the magnetic parameter causes a decrease in skin friction but an increase in Nusselt number.
- When Rd varies from 0.1 to 0.4, the heat transfer raises up to 35%.
- As the intensity of thermal radiation rises, the Nusselt number exhibits a corresponding increase.
- Augmenting the Stefan blowing number leads to an increase in skin friction, coupled with a decrease in the Nusselt number and Sherwood number.

- The generation of entropy is enhanced as the Eckert number and diffusion parameter are increased.

Author Contributions: Conceptualization, J.K. and S.S.; methodology, J.K.; software, J.K. and V.S.R.; validation J.K.; formal analysis, J.K., S.S. and V.S.R.; investigation, J.K.; resources, J.K.; writing—original draft preparation, J.K. and V.S.R.; writing—review and editing, J.K.; visualization, J.K.; supervision, J.K. All authors have read and agreed to the published version of the manuscript.

Funding: This research received no external funding.

Data Availability Statement: Not applicable.

Conflicts of Interest: The authors declare no conflict of interest.

Nomenclature

| | |
|------------|---|
| Sb | Stefan blowing parameter |
| B_0 | Magnetic field strength |
| u, v | velocity components along x and r directions |
| c | needle radius (m) |
| T_∞ | ambient temperature (K) |
| C_w | wall concentration |
| Nu_x | Nusselt number |
| C_∞ | ambient concentration |
| U_w | velocity at the surface (m s^{-1}) |
| σ^* | Stefan-Boltzman Constant |
| T_w | temperature at the surface (K) |
| C_p | specific heat ($\text{kg}^{-1} \text{J}$) |
| U_∞ | free stream velocity (m s^{-1}) |
| q_r | radiative heat flux ($\text{kg m}^2 \text{s}^{-3}$) |
| C_f | Skin friction |
| Sh_x | Sherwood number |
| D_m | mass diffusion coefficient ($\text{m}^2 \text{s}^{-1}$) |
| k^* | coefficient of mean absorption (c m^{-1}) |
| C | fluid concentration |
| Re_x | Local Reynolds number |

Greek Symbols

| | |
|---------------|------------------------------|
| ε | velocity ratio |
| ν | kinematic viscosity |
| ρ | fluid density |
| μ | dynamic viscosity of a fluid |

Subscripts

| | |
|-------|------------------|
| nf | nanofluid |
| f | fluid |
| hnf | hybrid nanofluid |

References

1. Siti Khuzaimah, S.; Anuar, I.; Ioan, P. Boundary layer flow past a continuously moving thin needle in a nanofluid. *Appl. Therm. Eng.* **2016**, *114*, 58–64.
2. Ghadikolaei, S.S.; Yassari, M.; Sadeghi, H.; Hosseinzadeh, K.; Ganji, D.D. Investigation on thermophysical properties of $\text{TiO}_2\text{-Cu}/\text{H}_2\text{O}$ hybrid nanofluid transport dependent on shape factor in MHD stagnation point flow. *Powder Technol.* **2017**, *322*, 425–438. [[CrossRef](#)]
3. Siti Nur, A.S.; Norfifah, B.; Norihan, M.A.; Ioan, P. Stability analysis of mixed convection flow towards a moving thin needle in nanofluid. *Appl. Sci.* **2018**, *8*, 842.
4. Iskandar, W.; Anuar, I.; Ioan, P. Hybrid nanofluid flow past a permeable moving thin needle. *Mathematics* **2020**, *8*, 612.
5. Hassan, W.; Syed Muhammad Raza, S.N.; Alqarni, M.S.; Muhammad, T. Thermal transport in magnetized flow of hybrid nanofluids over a vertical stretching cylinder. *Case Stud. Therm. Eng.* **2021**, *27*, 101–219.
6. Zainal, N.A.; Roslinda, N.; Kohilavani, N.; Ioan, P. Steady analysis of unsteady hybrid nanofluid flow past a permeable stretching/shrinking cylinder. *J. Adv. Res. Fluid Mech. Therm. Sci.* **2021**, *86*, 64–75. [[CrossRef](#)]

7. Sivasankaran, S.; Narrein, K. Numerical investigation of two-phase laminar pulsating nanofluid flow in helical microchannel filled with a porous medium. *Int. Commun. Heat Mass Transf.* **2016**, *75*, 86–91. [[CrossRef](#)]
8. Sivasankaran, S.; Bhuvanewari, M. Numerical study on influence of water based hybrid nanofluid and porous media on heat transfer and pressure loss. *Case Stud. Therm. Eng.* **2022**, *34*, 102022. [[CrossRef](#)]
9. Sivasankaran, S.; Pan, K.L. Natural convection of nanofluids in a cavity with nonuniform temperature distributions on side walls. *Numer. Heat Transf.* **2014**, *65*, 247–268. [[CrossRef](#)]
10. Sivasankaran, S.; Chandrapushpam, T.; Bhuvanewari, M.; Karthikeyan, S. Effect of chemical reaction on double diffusive MHD squeezing copper water nanofluid flow between parallel plates. *J. Mol. Liq.* **2022**, *368*, 120768. [[CrossRef](#)]
11. Sivasankaran, S.; Bhuvanewari, M.; Alzahrani, A.K. Numerical study on influence of magnetic field and discrete heating on free convection in a porous container. *Sci. Iran. Trans. Mech. Eng. B* **2022**, *29*, 3063–3071.
12. Bhuvanewari, M.; Sivasankaran, S.; Kim, Y.J. Magnetoconvection in a square enclosure with sinusoidal temperature distributions on both side walls. *Numer. Heat Transf. Part A Appl.* **2011**, *59*, 167–184. [[CrossRef](#)]
13. Sivasankaran, S.; Niranjan, H.; Bhuvanewari, M. Chemical reaction, radiation and slip effects on MHD mixed convection stagnation-point flow in a porous medium with convective boundary condition. *Int. J. Numer. Methods Heat Fluid Flow* **2017**, *27*, 454–470. [[CrossRef](#)]
14. Sivanandam, S.; Marimuthu, B. Numerical study on influence of inclination and sinusoidal heating on magneto-convection in an inclined lid-driven cavity. *Multidiscip. Model. Mater. Struct.* **2023**, *19*, 361–374. [[CrossRef](#)]
15. Sulochana, C.; Samrat, S.P.; Sandeep, N. Boundary layer analysis of an incessant moving needle in MHD radiative nanofluid with Joule heating. *Int. J. Mech. Sci.* **2017**, *128*, 326–331. [[CrossRef](#)]
16. Eswarmoothi, S.; Jagan, K.; Sivasankaran, S. MHD bioconvective flow of a thermally radiative nano liquid in a stratified medium considering gyrotactic microorganisms. *J. Phys.* **2020**, *1597*, 012001.
17. Umair, K.; Zaib, A.; Khan, I.; Dumitru, B.; El-Sayed, M.S. Comparative investigation on MHD nonlinear radiative flow through a moving thin needle comprising two hybridized AA7075 and AA7072 alloys nanomaterials through binary chemical reaction with activation energy. *J. Mater. Res. Technol.* **2020**, *9*, 3817–3828.
18. Iskander, T.; Hossaam, A.; Nabwey, M.; Girinath Reddy, N.; Sandeep; Maddileti, P. Effect of resistive heating on incessant poignant thin needle in magnetohydrodynamics Sakiadis hybrid nanofluid. *Ain Shams Eng. J.* **2021**, *12*, 1025–1032.
19. Reddy, V.S.; Jagan, K.; Sivanandam, S. Impacts of Casson Model on Hybrid Nanofluid Flow over a Moving Thin Needle with Dufour and Soret and Thermal Radiation Effects. *Math. Comput. Appl.* **2023**, *28*, 2. [[CrossRef](#)]
20. Sivasankaran, S.; Bhuvanewari, M.; Amer, A.A. Numerical study on buoyant convection and thermal radiation in a cavity with various thermal sources and Cattaneo–Christov heat flux. *Case Stud. Therm. Eng.* **2021**, *27*, 101207. [[CrossRef](#)]
21. Sivasankaran, S.; Bhuvanewari, M.; Alzahrani, A.K. Numerical simulation on convection of non-Newtonian fluid in a porous enclosure with non-uniform heating and thermal radiation. *Alex. Eng. J.* **2020**, *59*, 3315–3323. [[CrossRef](#)]
22. Karthikeyan, S.; Bhuvanewari, M.; Sivasankaran, S.; Rajan, S. Soret and Dufour effects on MHD mixed convection heat and mass transfer of a stagnation point flow towards a vertical plate in a porous medium with chemical reaction, radiation and heat generation. *J. Appl. Fluid Mech.* **2016**, *9*, 1447–1455. [[CrossRef](#)]
23. Niranjan, H.; Sivasankaran, S.; Bhuvanewari, M. Chemical reaction, Soret and Dufour effects on MHD mixed convection stagnation point flow with radiation and slip condition. *Sci. Iran.* **2017**, *24*, 698–706. [[CrossRef](#)]
24. Muhammed, I.A.; Iskander, T.; Muhammed, Q.; Ilyas, K. Nonlinear Roseland thermal radiation and energy dissipation effects on entropy generation in CNTs suspended nanofluids flow over a thin needle. *Bound. Value Probl.* **2018**, *148*, 1–14.
25. Himanshu, U.; Manoj, K. Influence of non-linear radiation, Joule heating and viscous dissipation on the boundary layer flow of MHD nanofluid flow over a thin moving needle. *Multidiscip. Model. Mater. Struct.* **2020**, *16*, 208–224.
26. Sreedevi, P.; Sudarsana, R. Impact of Convective Boundary Condition on Heat and mass transfer of nanofluid flow over a thin needle filled with Carbon nanotubes. *J. Nanofluids* **2020**, *9*, 282–292. [[CrossRef](#)]
27. Puneeth, V.; Manjunath, S.; Makinde, O.D.; Gireesha, B.J. Bioconvection of a Radiating Hybrid Nanofluid Past a Thin Needle in the Presence of Heterogeneous–Homogeneous Chemical Reaction. *J. Heat Trans.* **2021**, *143*, 042502. [[CrossRef](#)]
28. Haider, S.M.A.; Bagh, A.; Qiuwang, W.; Cunlu, Z. Stefan Blowing Impacts on Unsteady MHD Flow of Nanofluid over a Stretching Sheet with Electric Field, Thermal Radiation and Activation Energy. *Coatings* **2021**, *11*, 1048. [[CrossRef](#)]
29. Narayanaswamy, M.K.; Kandasamy, J.; Sivanandam, S. Go-MoS₂/Water Flow over a Shrinking Cylinder with Stefan Blowing, Joule Heating, and Thermal Radiation. *Math. Comput. Appl.* **2022**, *27*, 110. [[CrossRef](#)]
30. Tiegang, F.; Wei, J. Flow, heat and species transfer over a stretching plate considering coupled Stefan blowing effects from species transfer. *Commun. Nonlinear Sci. Numer. Simulat.* **2014**, *19*, 3086–3097.
31. Shib Sankar, G.; Kalidas, D.; Prabir Kumar, K. Stefan blowing effects on MHD biconvection flow of a nanofluid in the presence of gyrotactic microorganisms with active and passive nanoparticles flux. *Eur. Phy. J. Plus* **2017**, *132*, 101.
32. Amirsom, N.A.; Mohammed, J.U.; Ismail, A.I.M. MHD boundary layer bionanoconvective non-Newtonian flow past a needle with Stefan blowing. *Heat Transfer Asian Res.* **2018**, *48*, 727–743. [[CrossRef](#)]
33. Jyothi, A.M.; Naveen Kumar, R.; Punith Gowda, R.J.; Prasannakumara, B.C. Significance of Stefan blowing effect in flow and heat transfer of Casson nanofluid over a moving thin needle. *Commun. Theor. Phys.* **2021**, *8*, 8. [[CrossRef](#)]
34. Narayanaswamy, M.N.; Kandasamy, J.; Sivasankaran, S. Impacts of Stefan Blowing on hybrid nanofluid flow over a stretching cylinder with thermal radiation and Dufour and Soret effect. *Math. Comput. Appl.* **2022**, *27*, 9. [[CrossRef](#)]

35. Muhammed, I.A.; Tlili, I.; Marjan, G.; Osman, M.; Najeeb, A.M. Irreversibility Analysis of Hybrid nanofluid flow over a thin needle with effects of energy dissipation. *Symmetry* **2019**, *11*, 663.
36. Iskander, T.; Muhammed, R.; Kadry, S.; Hyun-Woo, K.; Yunyoung, N. Radiative Nanofluid flow over a moving thin needle with Entropy generation in a porous medium with Dust particles and Hall current. *Entropy* **2020**, *22*, 354.
37. Gangadhar, K.; Bhanu Lakshmi, K.; Kannan, T.; Ali, J.C. Entropy generation in magnetized Bioconvective nanofluid flow along a vertical cylinder with gyrotatic microorganisms. *J. Nanofluids* **2020**, *9*, 302–312. [[CrossRef](#)]
38. Muhammed, R.; Noor Saeed, K.; Poom, K. Mechanical analysis of non-Newtonian nanofluid past a thin needle with dipole effect and entropy characteristics. *Sci. Rep.* **2021**, *11*, 19378.
39. Ogunseye, H.A.; Agbaje, T.M.; Salawu, S.O.; Fatunmbi, E.O. A numerical study of entropy generation in dissipative and radiative Casson hybrid ferrofluid past a thin needle. *Res. Sq.* **2023**, 1–21. [[CrossRef](#)]
40. Jagan, K.; Sivasankaran, S. Three-Dimensional Non-Linearly Thermally Radiated Flow of Jeffrey Nanoliquid towards a Stretchy Surface with Convective Boundary and Cattaneo–Christov Flux. *Math. Comput. Appl.* **2022**, *27*, 98. [[CrossRef](#)]
41. Joyce, M.I.; Kandasamy, J.; Sivanandam, S. Entropy Generation of Cu–Al₂O₃/Water Flow with Convective Boundary Conditions through a Porous Stretching Sheet with Slip Effect, Joule Heating and Chemical Reaction. *Math. Comput. Appl.* **2023**, *28*, 18. [[CrossRef](#)]
42. Jagan, K.; Sivasankaran, S. Soret & Dufour and Triple Stratification Effect on MHD Flow with Velocity Slip towards a Stretching Cylinder. *Math. Comput. Appl.* **2022**, *27*, 25.

Disclaimer/Publisher’s Note: The statements, opinions and data contained in all publications are solely those of the individual author(s) and contributor(s) and not of MDPI and/or the editor(s). MDPI and/or the editor(s) disclaim responsibility for any injury to people or property resulting from any ideas, methods, instructions or products referred to in the content.